Supporting Information:

$Ni_{0.7}Co_{0.3}P$ nanoparticles loaded $MnCo_2S_4$ yolk-shell nanoflowers with Z-scheme heterojunction for efficient photocatalytic hydrogen evolution

Tingyang Li[a,c], Qian Liu[a,c], Zheng Xiong[a,b], Peng Ji[a,b], Ruiyang Zhao[a,c], Jishu Han[a,b]*, Lei Wang[a,b]**

[a]State Key Laboratory Base of Eco-chemical Engineering, International Science and Technology Cooperation Base of Eco-chemical Engineering and Green Manufacturing, Qingdao University of Science and Technology, Qingdao 266042, China. [b]College of Chemistry and Molecular Engineering, Qingdao University of Science and Technology, Qingdao 266042, China. [c]College of Chemical Engineering, Qingdao University of Science and Technology, Qingdao 266042, China.

Photocatalytic hydrogen production test

The catalytic process of photocatalysts was achieved in the online trace gas analysis system. Particularly, 100 mL of deionized water, 10 mg of photocatalyst, 33 mg of Eosin Y and 10 mL of TEOA were added into a 250 mL special designed transparent glass reactor. Throughout the entire experiment, Argon gas was served as the carrier gas and the reaction temperature was controlled at 6 ℃ by circulating cooling water. A 300 W Xenon lamp was placed above the glass container as light source, and magnetic stirrer was maintained at 500-600 r to ensure that the light was uniformly shone on the surface of the photocatalyst during the experiment. The test lasted for a total of 3 hours, a gas chromatograph was used to take samples every half an hour and recorded the amount of hydrogen production in the reactor.

Photoelectrochemical test

The photocurrent response test, electrochemical impedance test (EIS), and Mott-Schottky (M-S) test were carried out using an electrochemical workstation (CHI760E) and three-electrode system. In the three-electrode system, the Pt electrode and the Ag/AgCl electrode were used as the counter electrode and the reference electrode, respectively, while the working electrode was the FTO electrode coated with the sample. The electrolyte solution was 5 mol/L Na_2SO_4. 5 mg of sample powder was mixed with 10 μL of polytetrafluoroethylene and 300 μL of N-methyl pyrrolidone. Then the mixture was grinded for 30 min and coated on the FTO conductive glass sheet, and then dried to obtain the working electrode.

Characterization

The morphology and structure of the samples were analyzed by scanning electron microscopy (SEM, JSM-7900F, JEOL) and transmission electron microscopy (TEM, JEM-F200, JEOL). The X-ray diffraction (XRD) patterns were examined by the X-ray powder diffractometer (D/MAX/2500PC, Rigaku). The UV-visable diffuse reflectance spectra (UV-vis DRS) were investigated through the UV-Vis diffuse reflectance spectrometer (Agilent Cary 5000) to evaluate the optical absorption capacity of the sample. The electrochemical impedance spectra, photocurrent response spectra and Mot-Schottky curves were determined using the photoelectrochemical testing instrument (PEC-2000). Ultraviolet photoelectron spectroscopy (UPS) and X-ray photoelectron spectroscopy (XPS) analyses were conducted on the AXIS SUPRA instrument (Shimadzu). Steady-state photoluminescence spectra and time-resolved transient photoluminescence decay were studied using the FLS-1000 spectrometer (Edinburgh Instruments).

Table S1. The content of each element obtained by EDS measurement.

Element	P	S	Co	Mn	Ni
Mass Fraction (%)	11.42	35.41	41.34	5.06	6.78

Figure S1. XPS survey spectrum of $Ni_{0.7}Co_{0.3}P/MnCo_2S_4$.

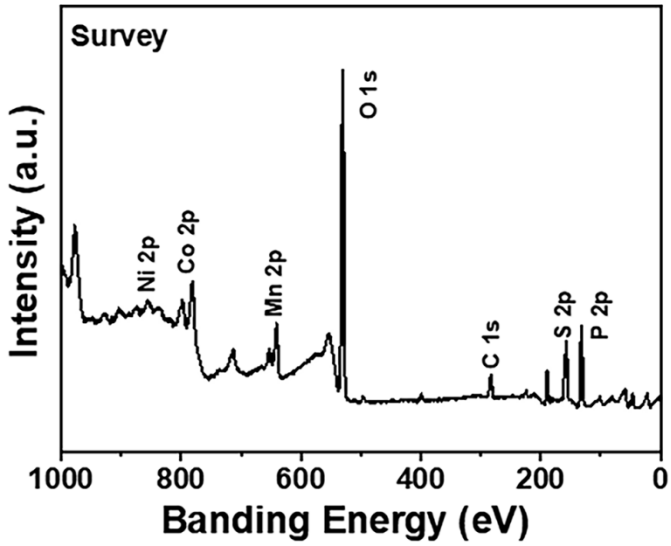

Figure S2. Photocatalytic hydrogen production efficiency of $Ni_{1-x}Co_xP$ and Ni_2P.

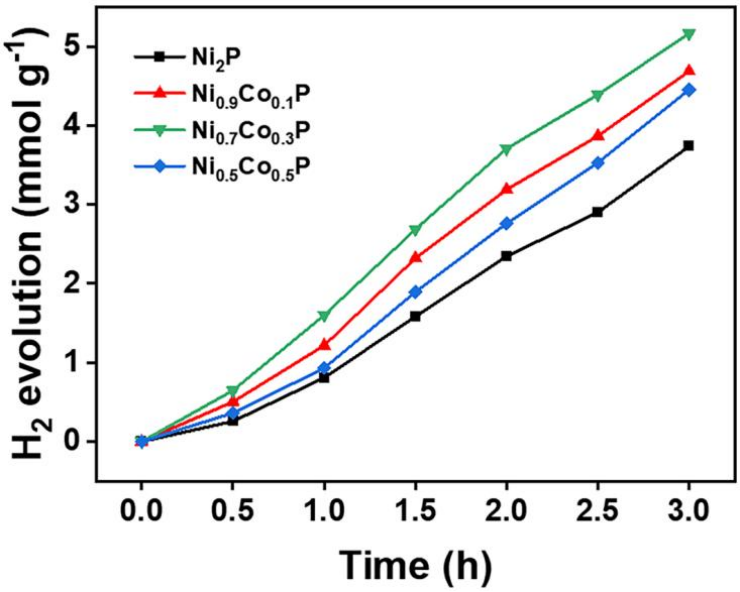

Figure S3. The SEM image of $Ni_{0.7}Co_{0.3}P/MnCo_2S_4$ after cyclic hydrogen production.

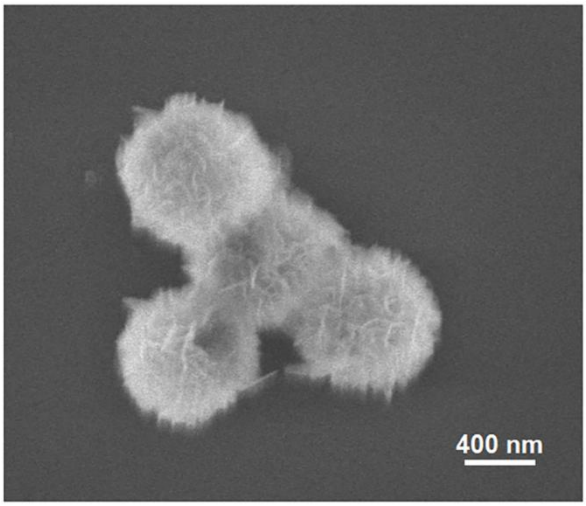

Figure S4. The influence of different concentrations of the photosensitizer on hydrogen production performance.

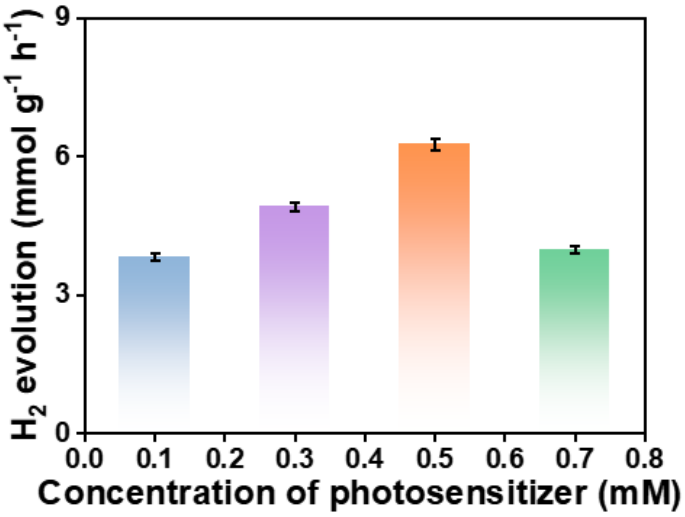

Table S2. Comparison of photocatalytic H_2 production performance of different catalysts.

Photocatalyst	H_2 production amount (mmol g^{-1})	Ref
$Ni_{0.7}Co_{0.3}P/MnCo_2S_4$	20.19	This work
$MnCo_2S_4/ZnIn_2S_4$	17.50	[1]
$CoS_2/MgIn_2S_4$	0.29	[2]
$ZnIn_2S_4/MnS$	7.95	[3]
$NiCoP/ZnIn_2S_4$	3.84	[4]
ZnCdS/NiCoP	1.37	[5]
CdS/MnS	5.92	[6]
$NiCoP/TiO_2/g\text{-}C_3N_4$	2.31	[7]
$NiCoP/Cu_3P$	8.90	[8]
$2\%Ni_{0.1}Co_{0.9}P\text{-}ZnIn_2S_4$	3.84	[9]
$Ni_2P/g\text{-}C_3N_4$	0.22	[10]
$NiCoP/CdIn_2S_4$	0.65	[11]
$NiCoP/Zn_3In_2S_6$	18.70	[12]
$NiCo_2O_4/MnS/Mn_{0.2}Cd_{0.8}S$	3.31	[13]
MnS@ZnS	3.99	[14]
$Mn\text{-}CoS_x/CdS$	19.1	[15]
$MnCo_2S_4/Zn_3In_2S_6$	4.47	[16]

$MnCo_2S_4$/CdS	12.0	[17]
La-CoS, Gd-CoS	3.24, 2.91	[18]
NiCoP/ZnSe	4.27	[19]
NiCoP/g-C_3N_4	7.95	[20]

References

[1] Y. Xiao, J. Tian, H. Miao, E. Liu, Facile fabrication of S-scheme $MnCo_2S_4/ZnIn_2S_4$ heterojunction for photocatalytic H_2 evolution, Journal of Alloys and Compounds, 1003 (2024) 175636.

[2] J. Li, J. Yao, Q. Yu, X. Zhang, S. Carabinerio, X. Xiong, C. Wu, K. Lv, Understanding the unique Ohmic-junction for enhancing the photocatalytic activity of $CoS_2/MgIn_2S_4$ towards hydrogen production, Applied Catalysis B: Environment and Energy, 351 (2024) 123950.

[3] Y. Ma, Z. Feng, Y. Dong, Z. Yan, H. Wang, Y. Wu, Harnessing the interfacial sulfer-edge and metal-edge sites in $ZnIn_2S_4$/MnS heterojunctions boosts charge transfer for photocatalytic hydrogen production, Chinese Chemical Letters, 36 (2025) 110922.

[4] H. Song, S. Liu, Z. Sun, Y. Han, J. Xu, Y. Xu, J. Wu, H. Meng, X. Xu, T. Sun, X. Zhang, Rational design of direct Z-scheme heterostructure NiCoP/ZIS for highly efficient photocatalytic hydrogen evolution under visible light irradiation, Separation and Purification Technology, 275 (2021) 119153.

[5] J. Zhao, K. Li, H. She, Y. Zhang, J. Huang, L. Wang, F. Chen, Q. Wang, Highly efficient photocatalytic hydrogen production by ZnCdS composite catalyst modified with NiCoP nanosheets prepared by LDH precursor, Journal of Colloid and Interface Science, 649 (2023) 416-425.

[6] H. Zhang, Q. Feng, Y. Zhang, J. Zhang, X. Wu, Y. Li, L. Yin, J. Huang, X. Kong, A CdS/MnS p-n heterojunction with a directional carrier diffusion path for efficient photocatalytic H_2 production, Inorganic Chemistry Frontiers, 9 (2022) 1100-1106.

[7] X. Liu, L. Ma, X. Wang, X. Wu, B. Guo, L. Zhou, Z. Zhao, Structuring dual Z-scheme heterojunction and boosting surface reaction by bifunctional NiCoP Modified TiO_2/g-C_3N_4 for

improving the photocatalytic activity, International Journal of Hydrogen Energy, 62 (2024) 127-139.

[8] M. Yang, Y. Li, T. Yan, Z. Jin, NiCo LDH in situ derived NiCoP 3D nanoflowers coupled with a Cu_3P p-n heterojunction for efficient hydrogen evolution, Nanoscale, 13 (2021) 13858-13872.

[9] Y. Wang, T. Zhang, T. Wei, F. Li, L. Xu, Bimetallic phosphide $Ni_xCo_{1-x}P$ decorated flower-like $ZnIn_2S_4$ for enhanced photocatalytic hydrogen evolution, New Journal Chemistry, 45 (2021) 11261.

[10] Z. Wang, L. Li, M. Liu, T. Miao, X. Ye, S. Meng, S. Chen, X. Fu, A new phosphidation route for the synthesis of NiP_x and their cocatalytic performances for photocatalytic hydrogen evolution over g-C_3N_4, Journal of Energy Chemistry, 48 (2020) 241–249.

[11] H. Shi, E. Zhang, H. Zhu, H. Wang, A. Rong, L. Mao, NiCoP as a cocatalyst decorating $CdIn_2S_4$ for enhanced photocatalytic performance under visible light: DFT calculation and mechanism insight, International Journal of Hydrogen Energy, 51 (2024) 1287-1302.

[12] K. Su, W. Yin, X. Liu, S. Cai, P. He, Y. Xiao, T. Ren, Fabricating NiCoP/$Zn_3In_2S_6$ type II heterojunction photocatalyst for boosted photocatalytic hydrogen evolution performance, Inorganic Chemistry Communications, 178 (2025) 114488-114497.

[13] X. He, Q. Zeng, H. Zheng, W. Ong, Y. He, B. Huang, L. Li, D. Zeng, Insight into NiCo-based nanosheets modified MnS/$Mn_{0.2}Cd_{0.8}S$ hybrids for enhanced visible-light photocatalytic H_2 evolution, International Journal of Hydrogen Energy, 47 (2022) 13862-13875.

[14] C. Chang, C. Hung, J. Chen, C. Li, Y. Yu, Effects of surface property on loading octaaza bis-α-diimine Ni complex, charge separation, and H_2 production activity of MnS@ZnS photocatalysts, Surfaces and Interfaces, 48 (2024) 104253-104262.

[15] Y. Kong, K. Zhang, M. Gu, Y. Zhang, J. Huang, F. Luo, Y. Feng, Manganese-doped amorphous core-shell cobaltous sulfide for enhanced photocatalytic hydrogen evolution, International Journal of Hydrogen Energy, 160 (2025) 150621-150630.

[16] S. Zhang, L. Zhang, F. Yue, Y. Meng, M. Shi, C. Li, W. Li, X. Qian, Y. Ma, L. Wang, H. Zhang, Novel cocatalyst $MnCo_2S_4$ based on $Zn_3In_2S_6$ for enhanced photocatalytic hydrogen production and ranitidine degradation, Journal of Alloys and Compounds, 1004 (2024) 175941-175950.

[17] Y. Cheng, M. Dou, M. Yao, K. Ding, H. Shao, Y. Liu, S. Li, Y. Chen, Reverse-type-I $MnCo_2S_4$/CdS heterojunction nanorods for highly efficient photocatalytic hydrogen production under visible light irradiation, ACS Applied Nano Materials, 6 (2023) 16837-16845.

[18] W. Wang, Z. Zhang, J. Ying, L. Cao, X. Chen, K. Wei, L. Gou, E. Liu, Metal organic framework derived La/Gd-doped CoS for enhanced photocatalytic H_2 evolution, Colloids and Surfaces A: Physicochemical and Engineering Aspects, 685 (2024) 133219-133228.

[19] Q. Zeng, Y. Tan, X. Yin, G. Gao, C. He, Y. Wei, D. Zeng, Engineering NiCoP nanosheet/ZnSe nanoparticle heterostructures for enhanced photocatalytic hydrogen production, Chemical Communications, 61 (2025) 9063-9066.

[20] Y. Chen, J. Ma, J. Fu, L. Sun, J. Cheng, J. Li, Enhanced photocatalytic hydrogen evolution over protonated g-C_3N_4 using NiCoP as a cocatalyst, International Journal of Hydrogen Energy, 51 (2024) 1145-1152.

Table S3. Life-span calculation parameters of $MnCo_2S_4$, $Ni_{0.7}Co_{0.3}P$ and $Ni_{0.7}Co_{0.3}P/MnCo_2S_4$.

Samples	A_1	τ_1 (ns)	A_2	τ_2 (ns)	τ_{ave} (ns)
$MnCo_2S_4$	0.99	1.09	0.07	4.11	1.74
$Ni_{0.7}Co_{0.3}P$	0.94	1.02	0.09	3.78	1.73
$Ni_{0.7}Co_{0.3}P/MnCo_2S_4$	1.12	1.09	0.04	6.89	2.05

The time-resolved transient PL decay curves of $MnCo_2S_4$, $Ni_{0.7}Co_{0.3}P$ and $Ni_{0.7}Co_{0.3}P/MnCo_2S_4$ were fitted at first. In our experiment, all the decay curves followed a double-exponential kinetic function fitting model (The equation was $I = A_1e^{-\frac{t}{\tau_1}} + A_2e^{-\frac{t}{\tau_2}}$). And all the fittings had close-to-unity coefficient of determination (R^2), implying high goodness-of-fit for the model. The average lifetime (τ_{ave}) of the samples were calculated through the equation $\tau_{ave} = \frac{A_1\tau_1^2+A_2\tau_2^2}{A_1\tau_1+A_2\tau_2}$.